Pharmaceutical Research, Vol. 22, No. 8, August 2005 (© 2005)
DOI: 10.1007/s11095-005-5274-8

Research Paper

Development of Stably Transfected Monolayer Overexpressing the Human Apical Sodium-Dependent Bile Acid Transporter (hASBT)

Anand Balakrishnan,[1] Daniel J. Sussman,[1,2] and James E. Polli[1,3]

Received December 30, 2004; accepted April 4, 2005

Purpose. The human apical sodium-dependent bile acid transporter (hASBT) represents a potential target for prodrug design to increase oral drug absorption. Unfortunately, available monolayer cell culture models do not reliably express hASBT, and nonpolarized cells only allow for uptake assessment, which limits prodrug development efforts. The objective of this study was to develop and characterize a stably transfected hASBT–MDCK cell line.

Methods. cDNA encoding hASBT was cloned into pcDNA3.1–V5-polyHis-B to generate an expression plasmid that was then transfected into MDCK-II cells. Clonal populations were chosen based on high hASBT activity and monolayer integrity. Western blot confirmed the expression of the recombinant hASBT; functionality was characterized using taurocholic acid.

Results. In the selected clone, hASBT-mediated taurocholate permeability across hASBT–MDCK monolayers was almost 25-fold higher with sodium, than without sodium where hASBT is not functional. In the presence of sodium, taurocholate and mannitol permeabilities were 23.0×10^{-6} cm/sec and 2.60×10^{-6} cm/s, respectively, indicating high hASBT functionality and monolayer integrity. hASBT-MDCK monolayer properties were stable over 6 months and demonstrated low within-day variability. Taurocholate uptake and inhibition kinetic parameters from hASBT–MDCK were similar to those obtained from hASBT–COS7 model, confirming hASBT functionality in hASBT-MDCK.

Conclusions. Results indicate that the developed hASBT–MDCK system is a competent, high-expression, stable assay for hASBT transport and inhibition studies.

KEY WORDS: ASBT; bile acid; cell culture, prodrug; transporter.

INTRODUCTION

The small intestine expresses many membrane transport proteins that translocate nutrients, xenobiotics, metabolites, and cell signaling moieties (1,2). These influx transporters represent potential targets to enhance the intestinal absorption of drugs and prodrugs. For example, the proton-coupled peptide transport system has been successfully targeted to increase drug absorption via a prodrug approach (3). The human apical sodium-dependent bile acid transporter (hASBT) is another potential target, particularly since hASBT possesses high transport efficiency and capacity. However, hASBT has not been well explored as a target to enhance oral drug or prodrug absorption, although a bile acid conjugate of acyclovir enhanced oral acyclovir absorption in rats (4).

Two related reasons for the lack of progress appear to be a poor understanding of the substrate requirements of hASBT (5,6) and the unavailability of an effective and convenient assay system to measure hASBT-mediated transport. Current cell culture assays employ nonpolarized cells, such as transiently transfected COS7 cells and stably transfected Chinese hamster ovary (CHO) cells. These models allow for uptake assessment, but are not competent monolayers and do not allow for transepithelial transport. In particular, previous studies from our laboratory employed uptake studies of an acyclovir prodrug using hASBT–COS7 cells. The cell lysis procedure complicated analysis of this bile acid prodrug, because of hydrolysis of prodrug to acyclovir (4). A monolayer model would be significantly beneficial because it would allow the measurement of prodrug transport, including quantification of intact prodrug in the receiver compartment. Also, the analytical requirements for a monolayer assay are generally less complex since the sample mat-

[1] Department of Pharmaceutical Sciences, School of Pharmacy, University of Maryland, Baltimore, Maryland 21201, USA.
[2] Present address: NCI Division of Cancer Biology, Tumor Biology and Metastasis Branch, Rockville, Maryland 20892, USA.
[3] To whom correspondence should be addressed. (e-mail: jpolli@rx.umaryland.edu)

ABBREVIATIONS: BSA, bovine serum albumin; CA, cholic acid; CDCA, chenodeoxycholic acid; DAPI, 4′,6-diamidino-2-phenylindole; DCA, deoxycholic acid; DIDS, 4,4′-diisothiocyanostilbene-2,2′-disulfonic acid; DMEM, Dulbecco's modified Eagle medium; GCA, glycocholic acid; GCDCA, glycochenodeoxycholic acid; GDCA, glycodeoxycholic acid; hASBT, human apical sodium-dependent bile acid transporter; HBSS, Hank's balanced salt solution; MDCK, Madin-Darby canine kidney; MRP, multidrug resistance-associated protein; OATP, organic anion transport peptide; PBS, phosphate-buffered saline; SLC, solute carrier family; TCA, taurocholic acid; TCDCA, taurochenodeoxycholic acid; TDCA, taurodeoxycholic acid; UDCA, ursodeoxycholic acid.

rix is relatively clean buffer compared to cell lysate in case of uptake. A monolayer system that overexpresses hASBT, without expressing confounding transporters, would significantly facilitate the elucidation of hASBT substrate requirements and efforts to exploit hASBT for drug delivery.

The objective of this study was to develop and characterize a stably transfected hASBT–MDCK cell line. Madin-Darby canine kidney (MDCK) type 2 cells were chosen since they are a polarized, epithelial cell line that grows as a competent monolayer and amenable to stable transfection. These cells have been used to successfully express other solute carrier (SLC) proteins (7). The developed hASBT–MDCK cell line was characterized with regard to hASBT expression, as well as hASBT-mediated transport and inhibition. Functionality of recombinant hASBT was characterized using taurocholic acid as a model substrate. Kinetic parameters of taurocholate uptake and inhibition from hASBT–MDCK were compared to the previously established hASBT–COS model. hASBT–MDCK monolayer integrity was measured using mannitol. Results indicate that the developed hASBT–MDCK system is a competent, high-expressing, stable assay for hASBT transport and inhibition that is expected to be useful in subsequent efforts to delineate the substrate requirements of hASBT, including prodrug strategies to exploit hASBT.

MATERIALS AND METHODS

Materials

Platinum® Taq DNA Polymerase, subcloning efficiency DH-5α competent cells, neomycin, fetal bovine serum, trypsin, Lipofectamine 2000, pcDNA 3.1-V5-His, Dulbecco's modified Eagle medium (DMEM), antiV5-HRP antibody, and Alexa Fluor 488 goat anti-mouse antibody were purchased from Invitrogen Corporation (Carlsbad, CA). COS7 cells were purchased from ATCC (Manassas, VA). 4′,6-Diamidino-2-phenylindole (DAPI) was obtained from Roche-Boehringer Mannheim (Mannheim, Germany). [^{14}C]mannitol was purchased from Moravek Biochemicals (Brea, CA). [^{3}H]Taurocholic acid was acquired from NEN PerkinElmer (Boston, MA). DNA isolation kits were sourced from Qiagen (Valencia, CA). All other chemicals were obtained from Sigma Chemical (St. Louis, MO) or TCI America (Portland, OR).

Construction and Evaluation of Expression System

hASBT cDNA subcloned into the mammalian expression vector pCMV2 was kindly donated by Paul Dawson (Wake Forest University). hASBT cDNA was amplified from the pCMV plasmid by polymerase chain reaction (PCR) using Platinum® Taq DNA Polymerase with appropriate primers [5′ TTG ACG CAA ATG GGC GGT AG (sense) and 5′GCC CTC TAG ACA CTT TTC GTC AGG TTG AAA (antisense)]. hASBT cDNA was cloned into a pcDNA3.1 expression system that allows recombinant hASBT expression and selection of transfected cells using neomycin resistance. The *Xba*I restriction site was introduced in the primers for ease of cloning. The stop codon was omitted to allow the expression of the V5-His epitope down stream of the hASBT sequence. The expression plasmid was transformed into DH-5α cells that were grown in Luria-Bertani medium (LB) broth agar plates containing 50 μg/ml of ampicillin as a selection agent. Positive clones were selected from the plates and expanded in 5 ml of LB broth containing ampicillin at 37°C. Plasmid DNA isolation and purification was carried out using a DNA isolation kit. Clones carrying the desired plasmid were screened based on southern blot to check for presence of full size plasmid and the size of the inserted hASBT sequence. Colonies carrying the full size insert were expanded and plasmid DNA isolated. The sequence of the inserted hASBT segment was verified using a fluorescence-based automated DNA sequencing system at the Biopolymer Core Facility (University of Maryland, Baltimore) and compared with the native coding sequence for hASBT in GenBank (Accession No. U67674). Functional evaluation of the expression system was checked by transient transfection into COS7 cells and hASBT-mediated taurocholic acid uptake (4).

Stable Transfection of hASBT into MDCK Monolayers

MDCK (type-II) cells were obtained from Dr. Joseph Polli (GlaxoSmithKline; Research Triangle Park, NC) and maintained in a humidified incubator at 37°C under 5% CO_2 atmosphere in complete DMEM supplemented with 10% (v/v) fetal bovine serum, 50 U/ml of penicillin, and 50 μg/ml of streptomycin. Cells were stably transfected using Lipofectamine 2000® using the manufacturer's instructions. Briefly, cells were plated at 8×10^6 cells/cm^2 in a 60-mm dish and transfected using 8 μg of pcDNA3.1-hASBT-V5-His per 60-mm dish on day 3. On day 4, transfected MDCK cells were split at ratios of 1:10 and 1:50 in fresh media. The transfected cells were selected by growth in 1000 μg/ml of G418 (Life Technologies; Carlsbad, CA). Viable cells under G418 selection yielded clonal cells by limiting dilution in 96-well plates. Clones were selected based on uptake and transport assays.

Western Blot

Confluent hASBT-MDCK and untransfected MDCK cells were lysed using lysis buffer (10 mM Tris-Cl, pH 7.4, 0.15 M NaCl, 5 mM EDTA, and 1% Triton X100). 100 μl/ml of protease cocktail inhibitor (Sigma-Aldrich; St. Louis, MO) was added to the lysate. Samples were frozen at –20°C. Samples were subsequently thawed and sonicated to completely solubilize lysate. Protein content was determined using commercially available Bio-Rad Dc protein assay kit. Protein fractions were separated using 4–20% gradient Ready Gels (Bio-Rad; Hercules, CA) and subsequently transblotted onto polyvinylidene fluoride (PVDF) membranes. The membranes were blocked in blocking buffer [5% powdered nonfat milk in phosphate-buffered saline (PBS) along with 0.05% Tween-80]. hASBT was detected using horseradish peroxidase-conjugated antibodies directed against the V-5 epitope on the recombinant hASBT. Lumi-GLO® chemiluminescence substrate system was used to detect the bands of interest on a Bio-Rad chemiluminescent imaging system.

Immunofluorescence

Cells were grown on four-chamber, tissue-treated glass slides (BD Biosciences; Bedford, MA) at a seeding density of 0.7 million cells per chamber and grown as described earlier. Cells were treated with 10 mM sodium butyrate for 15 h after 4 days to enhance hASBT expression. Subsequently, cells were washed three times with PBS and fixed for 20 min in 4% formaldehyde in PBS containing 4% sucrose followed by permeabilization in 0.2% Triton X-100 for 20 min. Nonspecific sites were blocked with bovine serum albumin (BSA). Murine primary antibody against V-5 was used at a dilution of 1:500 in the blocking buffer (1% BSA in PBS). After washing with blocking buffer for 30 min, cells were incubated with goat Alexaflour 488 anti-mouse antibodies (Molecular Probes; Eugene, OR) at 4 μg/ml. DAPI was used as a nuclear stain. After three washings with PBS, a glass cover slip was mounted on the cells using two drops of Gel Mount® (Biomedia; Foster City, CA) and sealed with transparent nail polish. Fluorescence was examined under Nikon T-2800 inverted microscope under 60× oil immersion objective.

Taurocholate Uptake

hASBT–MDCK cells were seeded at a density of 0.7 million cells/cm^2 in 12- well plates (Corning; Corning, NY). To enhance hASBT expression, cells were treated with 10 mM sodium butyrate for 12–15 h at 37°C prior to uptake study. Uptake buffer consisted of either Hank's balanced salts solution (HBSS) which contains 137 mM NaCl or a sodium-free, modified HBSS where sodium chloride was replaced with 137 mM tetraethylammonium chloride. Since bile acid transport is sodium dependent, studies using sodium-free buffer allowed for the measurement of passive uptake of bile acid.

To measure the kinetics of hASBT-mediated taurocholate uptake into hASBT–MDCK cells, uptake studies were performed at taurocholate concentrations ranging from 0.5 to 200 μM; donor solutions were spiked with [^{3}H]taurocholate. Cells were washed thrice with HBSS or modified HBSS and incubated with donor solutions at 37°C and 50 rpm for 10 min. Preliminary studies with samples collected at 5, 10, 15, 30, and 45 min showed that taurocholate uptake was linear over 10 min. The donor solution was removed and the cells were washed three times with chilled sodium free buffer. Cells were lysed using 0.25 ml of 1 N NaOH and neutralized with 0.25 ml of 1 N HCl. Cell lysate was then counted for associated radioactivity using a liquid scintillation counter (Beckman Instruments; Fullerton, CA). Protein content in each well was analyzed using the Bio-Rad Dc protein assay kit based on Lowry method. Data were analyzed in terms of V_{max} and K_m, as described later.

To characterize hASBT functionality in the developed hASBT–MDCK system, cis-inhibition studies of taurocholate uptake (0.5 μM) were carried out using individual native bile acids (0–100 μM). Cells were exposed to donor solution containing taurocholate and inhibitor for 10 min, as described earlier. Inhibition data was analyzed in terms of inhibition constant K_i, as described below. To confirm the role of hASBT in enhanced taurocholate uptake in the developed hASBT–MDCK system, hASBT–MDCK cells were exposed to various non-bile acid inhibitors (i.e., ouabain, 4, 4′-diisothiocyanostilbene-2,2′-disulfonic acid (DIDS), sodium azide, and probenecid) for 30 min prior to taurocholate uptake.

Taurocholate Transport Across hASBT Monolayers

Transport studies concern the translocation of taurocholate across a monolayer of hASBT–MDCK cells that are grown on a permeable filter support; uptake refers to the accumulation of taurocholate inside cells, which were grown on the bottom of plates, as described earlier. In transport studies, hASBT–MDCK cells were seeded at a density of 0.75 million cells/cm^2 on polyester Transwells (Corning; Corning, NY, 0.4 μm pore size, 1 cm^2) and grown under otherwise identical conditions described earlier for uptake studies. Cells were washed three times with HBSS or modified HBSS prior to transport study and studies were carried out at 37°C at 50 rpm using an orbital shaker.

Taurocholate flux in both the apical-to-basolateral (A–B) and basolateral-to-apical (B–A) directions was measured using [^{3}H]taurocholic acid. Also, kinetics of hASBT-mediated taurocholate flux was assessed from transport studies conducted at different donor concentrations (1–200 μM spiked with [^{3}H]taurocholate). In all studies, [^{14}C]mannitol was used to monitor monolayer integrity. The apical and basolateral volumes were 0.5 ml and 1.5 ml, respectively. Samples were collected at multiple time points for at least 120 min and assessed for steady-state kinetics. All subsequent studies were single time point studies at 60 min. The amount of taurocholate transported was quantified using scintillation counting. Mass balance ranged between 85% and 110%.

Kinetic Analysis

Uptake and transport studies were performed in the presence and absence of sodium, as hASBT is a sodium-dependent transporter. Data from sodium-free studies were fitted to the following model to calculate the passive component:

$$\frac{dM}{dt} = P_p \cdot S \tag{1}$$

where dM/dt refers to the amount transported per unit time (and per unit area for transport studies), S is taurocholate concentration, and P_p is the passive uptake/transport rate constant.

Data from HBSS studies (i.e., sodium-containing studies) were fitted to the following modified Michaelis-Menten model:

$$\frac{dM}{dt} = \frac{V_{max} \cdot S}{K_m + S} + P_p \cdot S \tag{2}$$

where V_{max} and K_m represent the Michaelis-Menten constants for hASBT functioning. Equation (2) is composed of a nonlinear, Michaelis-Menten component, as well as linear, passive uptake/transport component.

Data analysis considered various approaches of normalizing taurocholate uptake (i.e., normalization with respect to area and with respect to protein). Normalizing against

protein did not provide any benefit to the uptake data, but rather introduced additional error because of variability in protein estimation (data not shown). Normalizing with respect to area did not add variability. Moreover, each of the normalization approaches provided similar relative estimation error which supports the lack of need to normalize against protein content.

Data analysis also evaluated two approaches to estimate V_{max} and K_m were examined. In one approach (i.e., first approach), passive uptake (P_p) was first estimated from sodium-free studies [Eq. (1)] and subsequently applied in Eq. (2) to analyze data from HBSS studies to estimate V_{max} and K_m. The second approach did not employ sodium-free data, but rather estimated V_{max}, K_m, and P_p simultaneously using Eq. (2) from HBSS studies.

The following competitive inhibition model was applied to cis-inhibition studies of taurocholate uptake by individual bile acids:

$$\frac{dM}{dt} = \frac{V_{max} \cdot S}{K_m\left(1 + \frac{I}{K_i}\right) + S} + P_p \cdot S \qquad (3)$$

where I is the concentration of inhibitor (i.e., inhibitory bile acid) and S is the concentration of taurocholate (i.e., 0.5 μM). In applying Eq. (3), only K_i was estimated. The other three parameters were estimated from taurocholate uptake studies without inhibitor. P_p was estimated from Eq. (1); V_{max} and K_m were estimated from Eq. (2).

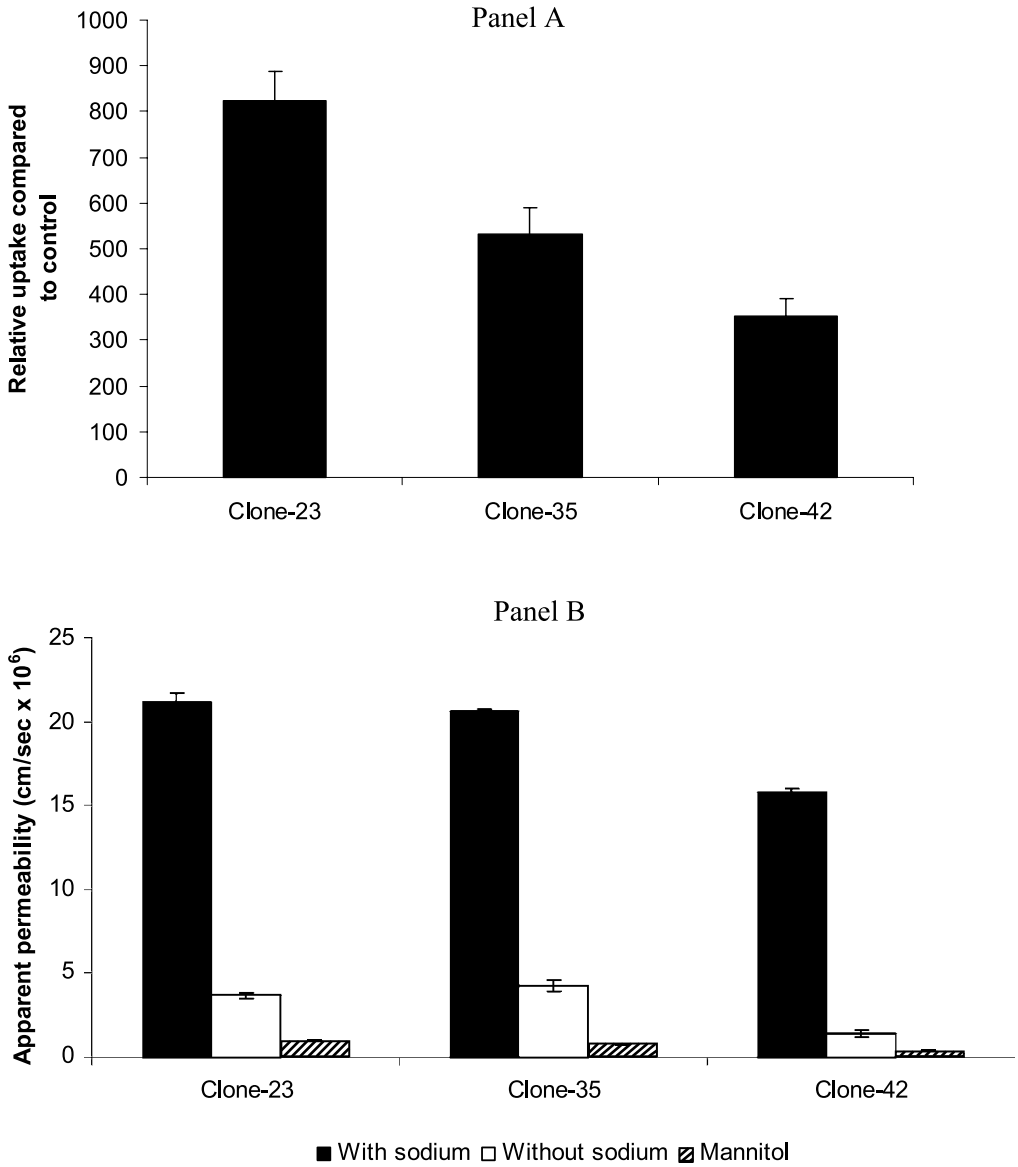

Fig. 1. Basis of clone selection. Although clones 23 and 35 had the highest hASBT expression levels, they were not chosen because of poor monolayer integrity. Clone 42 was selected because it exhibited both high functional expression and monolayer integrity. Panel A plots relative taurocholate uptake for three clones. Panel B illustrates apparent taurocholate permeability (with and without sodium) and mannitol for the three clones.

Statistical Analysis

Nonlinear curve fitting was performed using SigmaPlot2000 (SPSS version 6.0; Chicago, IL). Results were analyzed using Student's *t*-test and ANOVA. A p-value of less than 0.05 was considered significant. SEM of a ratio was calculated using the delta method (8).

RESULTS

Construction and Evaluation of hASBT Expression System

hASBT cDNA was cloned into the pcDNA3.1 expression vector, such that the V5-His epitope was inserted at the carboxy-terminus (see Materials and Methods). Southern blot and restriction digestion studies confirmed the presence of correct sized hASBT cDNA (data not shown). The inserted cDNA sequence was verified and found to share complete identity with the native coding sequence for hASBT reported in GenBank. Transient transfection of the expression plasmid in COS7 cells indicated functional expression of recombinant hASBT (data not shown).

Stable Transfection of hASBT into MDCK Monolayers

The hASBT expression vector was stably transfected into MDCK cells, as described in Materials and Methods. Among the 96 clonal populations that were screened for taurocholate uptake, three clones (clones 23, 35, and 42) were selected for further functional and biochemical evaluation (Fig. 1). In panel A of Fig. 1, each clone exhibited taurocholate uptake that was several hundred-fold higher, relative to sodium-free controls. In panel B of Fig. 1, apparent taurocholate permeability across hASBT–MDCK monolayer was high in each of the clones. It should be noted that the calculation of apparent permeability coefficient does not imply a passive permeability mechanism. Clone 42 was chosen for further consideration because this clone exhibited superior monolayer integrity based on mannitol permeability, as well as high hASBT expression and low passive taurocholate permeability. Clones 23 and 35 possessed higher hASBT activity than clone 42, but were less sensitive in transport assays than clone 42, owing to their lower monolayer integrity.

Recombinant hASBT was expressed in clone 42 in abundance as a single band at the expected molecular mass of approximately 42 kDa (Fig. 2). Confocal microscopy indicated hASBT expression in hASBT–MDCK cells (see Supplementary Fig. S1 available online at www.springerlink.com; search for DOI: 10.1007/s11095-005-5274-8; Electronic Supplementary Material can be found at the end of the article). hASBT was expressed at the apical membrane, but also seen in the cytosol. Untransfected MDCK cells essentially did not exhibit any florescence. Mock transfected MDCK cells, which were transfected with blank pcDNA3.1-V5-His vector, provided a low-level, diffuse fluorescence, as expected.

Kinetics of Taurocholate Uptake into hASBT-MDCK Cells

Figure 3 illustrates taurocholate uptake in hASBT–MDCK cells as a function of taurocholate concentration. In the presence of sodium, taurocholate exhibited non-linear, saturable uptake, reflecting translocation of taurocholate by hASBT across the apical membrane and into the cell. In the absence of sodium, taurocholate uptake was markedly reduced and linear with taurocholate concentration, reflecting only passive uptake. At the lowest concentration, taurocholate uptake in the presence of sodium was more than 100-fold higher than uptake in the absence of sodium. These results indicate high functional expression of hASBT.

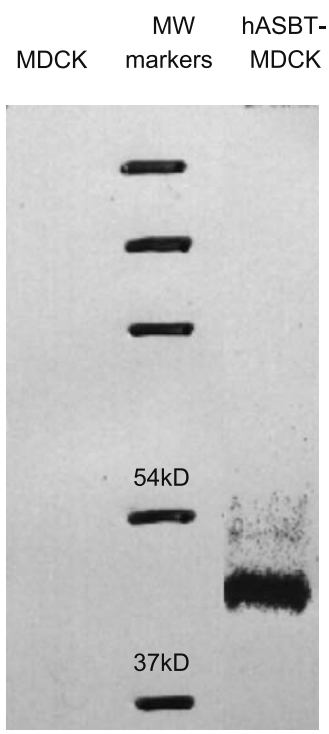

Fig. 2. Western blot. Lanes 1, 2, and 3 (left to right) show runs for untransfected MDCK cells, molecular weight markers, and hASBT–MDCK cells respectively. hASBT was detected in lane 3 as a single band with a molecular mass of approximately 42 kDa, indicating overexpression of hASBT.

Uptake was analyzed to estimate V_{max}, K_m, and P_p. Values of V_{max}, K_m, and P_p were 0.0208 (± 0.0008) nmol cm^{-2} min^{-1}, 7.27 (± 0.52) μM, and 1.88 (± 0.06) × 10^5 cm/min, respectively. It should be noted that the passive taurocholate uptake coefficient P_p was always about 10^{-5} cm/min, reflecting very low passive taurocholate uptake. These parameters were estimated in a two-step procedure (denoted the first approach in Materials and Methods), where P_p was estimated from sodium-free studies [Eq. (1)]; V_{max} and K_m were subsequently estimated from sodium-containing studies using Eq. (2). The appendix further discusses the performance of the two approaches to calculate V_{max}, K_m, and P_p.

Inhibition of Taurocholate Uptake into hASBT-MDCK Cells

Table I lists K_i values for the native bile acids for inhibition of taurocholate uptake into hASBT–MDCK, as well as hASBT–COS cells. K_i values were calculated using Eqs. (1), (2), and (3) as described in Materials and Methods. Each native bile acid inhibited taurocholate uptake in a dose-

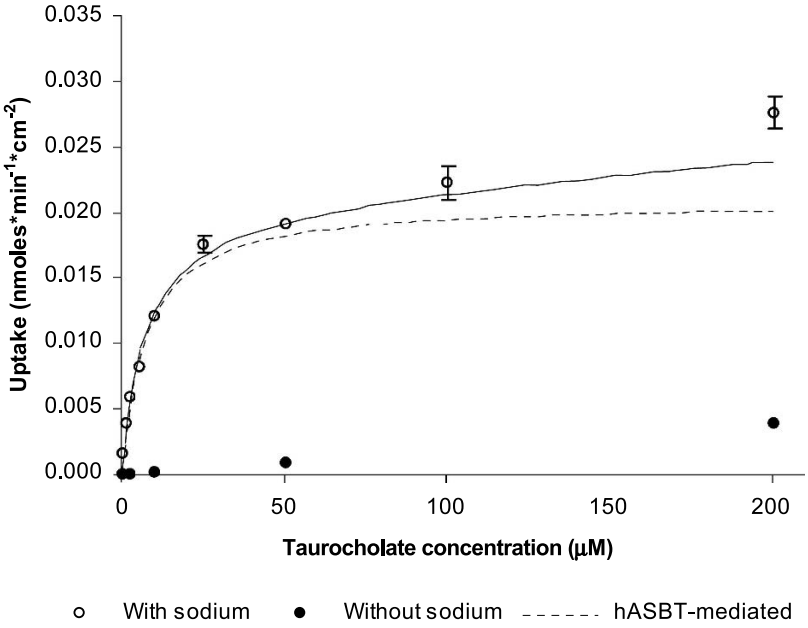

Fig. 3. Concentration-dependent uptake of taurocholate into hASBT–MDCK cells. Because hASBT is sodium dependent, taurocholate uptake was measured in the presence and absence of sodium. Uptake studies were performed at taurocholate concentrations ranging from 0.5 to 200 μM; donor solutions were spiked with [^{3}H]taurocholate. Cells were washed three times with HBSS or modified HBSS and incubated with donor solutions at 37°C and 50 rpm for 10 min. Studies in the absence of sodium assess passive uptake. The solid curve is the fit to total uptake data in the presence of sodium. The dashed line estimates hASBT-mediated uptake by subtracting passive uptake from total uptake.

dependent fashion. Figure 4 shows the concentration-dependent inhibition of taurocholate by glycochenodeoxycholic acid. Glycochenodeoxycholic acid concentration ranged from 0 to 100 μM, reducing taurocholate uptake 60-fold at the highest concentration. Similar profiles were observed for the other bile acids studied (data not shown).

In Table I, chenodeoxycholic acid and its conjugates exhibited the greatest affinities, with K_i values of about 2 μM in both hASBT–MDCK and hASBT–COS cells. Ursodeoxycholic acid possessed the weakest affinity in both the systems. In both the systems, hydroxylation pattern provided the following effect on K_i: chendeoxycholate < deoxycholate < cholate < ursodeoxycholate. In addition, glycine conjugation and taurine conjugation generally reduced K_i compared to unconjugated bile acids, and did so to about equal extents.

Four pharmacological modifiers were evaluated for their effect on taurocholate uptake in hASBT–MDCK cells. Compared to pharmacological modifier-free controls, taurocholate uptake was 9.92 (± 0.17)%, 140 (± 5)%, 124 (± 5)%, and 102 (± 3)% in the presence of ouabain, sodium azide, DIDS, and probenecid, respectively. A 90% reduction in hASBT-mediated taurocholate uptake was observed when hASBT–MDCK cells were pretreated with 100 μM ouabain. Ouabain is an inhibitor of Na^+,K^+-ATPase and abolishes the sodium gradient across the cell membrane, leading to inhibition of hASBT. Pretreatment with DIDS [anion-exchange inhibitor,

Table I. Inhibition Values (K_i) of Taurocholate Uptake by Native Bile Acids in hASBT–MDCK and hASBT-COS Cells[a]

Inhibitor	K_i (μM) from hASBT–MDCK uptake assay	K_i (μM) from hASBT–COS7 uptake assay[b]
Cholic acid	25.4 (± 1.3)	24.8 (± 5.1)
Glycocholic acid	11.0 (± 0.5)	20.6 (± 7.3)
Taurocholic acid	7.31 (± 0.26)	9.54 (± 1.19)
Chenodeoxycholic acid	3.34 (± 0.18)	1.28 (± 0.31)
Glycochenodeoxycholic acid	2.02 (± 0.17)	2.86 (± 0.17)
Taurochenodeoxycholic acid	2.09 (± 0.16)	0.99 (± 0.19)
Deoxycholic acid	12.9 (± 1.1)	5.16 (± 1.09)
Glycodeoxycholic acid	5.38 (± 0.39)	2.38 (± 0.36)
Taurodeoxycholic acid	4.99 (± 0.25)	4.54 (± 1.4)
Ursodeoxycholic acid	35.5 (± 2.2)	66.1 (± 10.9)

[a] Mean ± SEM (n = 3).
[b] Values from (4).

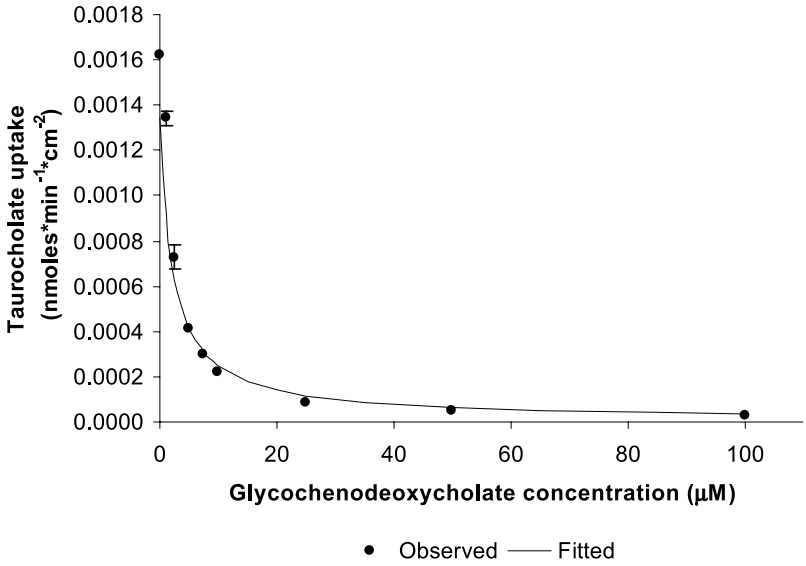

Fig. 4. Concentration-dependent inhibition of taurocholate uptake into hASBT–MDCK monolayers by glycochenodeoxycholic acid. Cis-inhibition studies of taurocholate uptake (0.5 μM) were carried out using individual native bile acids (0–100 μM). Cells were exposed to donor solution containing taurocholate and inhibitor for 10 min at 37°C. Qualitatively similar profiles were observed for each native bile acid.

including organic anion transporting peptide (OATP) inhibitor], sodium azide (metabolic inhibitor), or probenecid [multidrug resistance-associated protein (MRP) inhibitor] did not inhibit hASBT-mediated taurocholate uptake. No inhibition was observed in sodium-free studies, further indicating no modulation of taurocholate uptake by OATP or MRP. These results further support the role of hASBT in taurocholate uptake into hASBT–MDCK cells.

Comparison of Taurocholate Uptake Kinetics into hASBT-COS7 and hASBT–MDCK

Table II compares V_{max}, K_m, and P_p estimates for hASBT-mediated taurocholate uptake between the previously used hASBT–COS7 model and the newly developed hASBT–MDCK model. Both models yield similar estimates of K_m and P_p, and differed in V_{max}. This difference in V_{max} suggests a higher hASBT expression level in the hASBT–MDCK system, compared to the hASBT–COS7 system. Ideally, K_m is not expected to change since K_m parameterizes substrate affinity for the transporter. Because an hASBT antibody was not commercially available, the cytoplasmic tail of hASBT was tagged with a V5-His epitope. The addition of an epitope may compromise protein sorting and functionality (7). The similar K_m values across the systems suggests that the V5-His epitope in hASBT–MDCK did not modulate hASBT functioning.

Table II. Comparison of Taurocholate Uptake Parameters from hASBT–MDCK and hASBT–COS7 Assay Systems[a]

Parameter	hASBT–MDCK	hASBT–COS7[b]
V_{max} (nmol · $mg^{-1} \cdot min^{-1}$)	0.239 (± 0.008)	0.126 (± 0.006)
K_m (μM)	7.22 (± 0.44)	12.2 (± 2.2)
P_p (ml/min/mg) × 10^4	1.83 (± 0.06)	1.23 (± 0.05)

Estimates of K_m were each about 10 μM, indicating similar hASBT functioning across the two systems. Each system exhibited high V_{max} and low passive uptake (P_p).
[a] Mean ± SEM (n = 3).
[b] Values from (4).

K_i values from the native bile acid inhibition studies from hASBT were compared to those obtained previously from hASBT–COS7 assay (4). Table I illustrates the level of agreement in K_i values from these two systems. There was favorable agreement between the two assay systems (r^2 = 0.879). Taurocholate uptake and inhibition results indicate equivalency of hASBT functioning across the two assay systems, again supporting a lack of effect of the V5-His epitope in hASBT–MDCK.

Taurocholate Transport

Bidirectional transport studies showed polarized taurocholate transport, where apparent A–B permeability was more than 20-fold higher than apparent B–A permeability as seen in Fig. 5. Apparent taurocholate permeability was 26.8 (± 0.9) × 10^{-6} cm/s and 1.27 (± 0.04) × 10^{-6} cm/s in the A–B and B–A directions, respectively at taurocholate donor concentration of 0.5 μM. Figure 6 depicts the A–B transport of taurocholic acid across hASBT–MDCK monolayers in the presence and absence of sodium at varying concentrations of taurocholate. Taurocholate flux in the absence of sodium was considerably lower compared to studies in the presence of sodium.

Table III lists the apparent permeability of taurocholate and mannitol across hASBT–MDCK monolayers, mock transfected MDCK monolayers, and untransfected MDCK monolayers. A 23.7-fold difference in apparent taurocholate permeability between sodium-containing and sodium-free studies was observed for hASBT–MDCK cells. At 0.5 μM

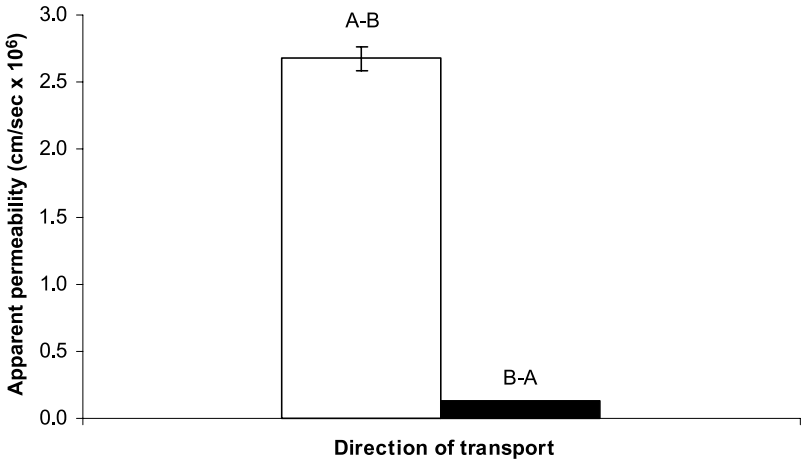

Fig. 5. Polarized transport of taurocholate across hASBT–MDCK monolayers. With a donor concentration of 0.5 μM, a 20-fold difference was observed between A–B and B–A apparent permeabilities.

taurocholate concentration, apparent taurocholate permeability across hASBT–MDCK was 18.7 (± 0.7) × 10^{-6} cm/s and 0.076 (± 0.06) × 10^{-6} cm/s in the presence and absence of sodium, respectively. Neither MDCK-II cells nor mock transfected cells exhibited sodium-dependent taurocholate transport. Mannitol and sodium-free taurocholate permeability values across these cells were comparable, indicating monolayer integrity of the hASBT–MDCK cell line.

In Fig. 6, taurocholate transport with sodium followed mixed Michaelis-Menten kinetics with both a saturable and a passive component. Table IV lists V_{max}, K_m, and P_p values for hASBT-mediated transport; kinetic parameters were estimated simultaneously using Eq. (2) (see Appendix). In Table IV, V_{max} and K_m were 937 (± 85) × 10^{-6} nmol s^{-1} cm^{-2} and 24.4 (± 3.7) μM, respectively. As observed in uptake studies (Fig. 4), taurocholate permeability in Fig. 6 was strongly sodium-dependent. At low taurocholate concentration, taurocholate permeability was 28-fold higher with sodium than without sodium. As expected, taurocholate exhibited a low passive monolayer permeability of 0.481 × 10^{-6} cm/s. Mannitol permeability was 2.10 (± 0.09) × 10^{-6} cm/s across all taurocholate concentrations reflecting hASBT– MDCK monolayer integrity.

Apparent taurocholate permeability was measured in the presence and absence of sodium on 10 different occasions over a 6-month period (see Supplementary Fig. S2 available online at www.springerlink.com; search for DOI: 10.1007/s11095-005-5274-8; Electronic Supplementary Material can be

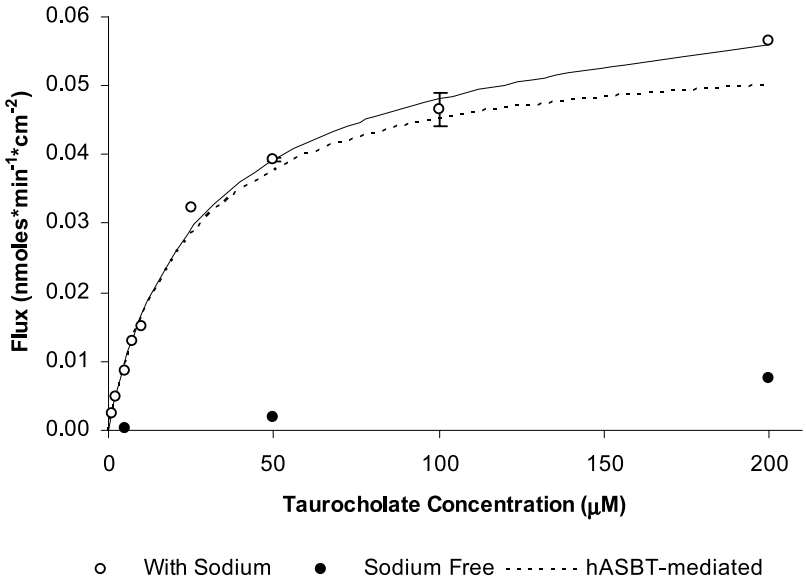

Fig. 6. Concentration-dependent transport of taurocholate across hASBT–MDCK monolayers in the A–B direction. Taurocholate flux was measured at varying concentrations of taurocholate (1–200 μM) in the presence and absence of sodium to delineate total and passive taurocholate flux. The solid curve is the fit to total flux data in the presence of sodium. The dashed line estimates hASBT-mediated flux by subtracting passive flux from total flux.

Table III. Comparison of Mannitol and Taurocholate Apparent Permeabilities Across Parent MDCK Monolayers, Mock Transfected Monolayers, and hASBT Transfected Monolayers[a]

Apparent permeability in A–B direction (cm/s × 10^6)	Parent MDCK	Mock transfected MDCK	hASBT–MDCK
Mannitol (without sodium)[b]	2.52 (± 0.07)	2.77 (± 0.25)	1.86 (± 0.04)
Taurocholate (with sodium)	0.843 (± 0.049)	0.819 (± 0.0002)	18.7 (± 0.7)
Taurocholate (without sodium)	1.14 (± 0.02)	0.840 (± 0.072)	0.789 (± 0.017)
Ratio of taurocholate permeability in presence and absence of sodium	0.740 (± 0.040)	0.980 (± 0.080)	23.7 (± 1.0)

hASBT–MDCK monolayers provided a 23.7-fold higher apparent taurocholate permeability in the presence of sodium, compared to sodium-free controls. Inclusion of sodium did not increase taurocholate permeability across either parent MDCK monolayers or mock transfected monolayers, indicating hASBT specifically mediated taurocholate transport. Mannitol permeabilities and passive taurocholate permeabilities from sodium-free studies were low and comparable across parent, mock transfected, and hASBT transfected systems.

[a] Mean ± SEM (n = 3).

[b] Mannitol permeability in the presence of sodium was essentially the same as mannitol permeability in the absence of sodium. Mannitol permeability with sodium was 1.79 (± 0.10), 2.07 (± 0.01), and 1.11 (± 0.09) × 10^{-6} cm/s across parent MDCK, mock transfected MDCK, and hASBT–MDCK monolayers, respectively.

found at the end of the article). Mannitol permeability was also evaluated. The mean apparent taurocholate permeability with sodium across all occasions was 22.8 (± 0.63) × 10^{-6} cm/s. The mean taurocholate permeability without sodium across all occasions was 1.29 (± 0.10) × 10^{-6} cm/s. In addition, the hASBT–MDCK model exhibited desirable monolayer integrity, as reflected by a mean mannitol permeability of 2.57 (± 0.20) × 10^{-6} cm/s.

Table V lists the within-day and between-day variabilities of taurocholate and mannitol permeabilities, as well as hASBT kinetic parameters. Within-day and between-day variability in apparent taurocholate permeability was assessed from studies using 0.5 μM taurocholate. Mannitol permeability was also assessed in each of these studies. Within-day variability was low for mannitol and taurocholate permeability in the presence and absence of sodium, with % coefficient of variation (%CV) less than 25%. Of note, the within-day %CV for taurocholate permeability with sodium was a favorable 6.2%. Also of note, the between-day variability in apparent taurocholate permeability with sodium was relatively low (%CV = 27.2%). Taurocholate permeability in the absence of sodium showed higher variability between days (%CV = 61.7%), as is typically the case for low-permeability solutes. Likewise, mannitol permeability also exhibited a higher between-day variability (%CV = 72.7). A positive correlation between mannitol permeability and passive permeability of taurocholate (r^2 = 0.784) suggests that the paracellular route may be the major transport pathway for the non-hASBT-mediated taurocholate transport.

Most importantly, these results reflect low within-day variability and relatively low between-day variability of apparent taurocholate permeability in the presence of sodium. The developed hASBT–MDCK system provided reproducible data within day, such that hASBT-mediated transport of two solutes can be conveniently measured and compared using a same-day study design. Apparent permeability values and kinetic parameters differed moderately between days (%CV typically 40–60%). Vmax exhibited a between day %CV = 57.2%, perhaps reflecting fluctuations in hASBT expression on different days. Higher V_{max} estimates tended to provide higher K_m estimates (data not shown).

Table IV. Kinetic Parameters of Taurocholate Transport Across hASBT–MDCK Monolayers in A–B Direction[a]

Parameter	Values (± SEM)
V_{max} (nmol · s^{-1} · cm^{-2} × 10^6)	937 (± 85)
K_m (μM)	24.4 (± 3.7)
P_p (cm/s × 10^6)	0.481 (± 0.368)

[a] Mean ± SEM (n = 3).

DISCUSSION

Also known as SLC10A2, hASBT is one of the important carrier proteins in the small intestine and is expressed in the terminal ileum. The transporter is electrogenic and needs sodium for its functioning, with 2:1 sodium:bile acid stoichiometry (9). Structural information on hASBT has been restricted to its primary sequence, membrane topology, and a three-dimensional homology-based model (10–12). hASBT contributes to the enterohepatic recirculation of native bile acids. The total bile acid pool in humans is about 3–5 g and enterohepatically recirculates about six times a day, leading to about 18 g of bile acid reabsorbed each day. In spite of this repeated recycling of bile acid, less than 0.5 g of bile acid is lost in the feces each day, reflecting hASBT's high capacity and efficiency (13). hASBT is quantitatively the dominant mechanism for bile acid absorption (5). Evidence for hASBT's importance is that primary bile acid malabsorption syndrome has been attributed to mutations in hASBT (14). Also, deletion of murine Asbt (Slc10a2) leads to complete disruption of bile acid recycling (15). We previously reported the successful targeting of ASBT to increase acyclovir oral bioavailability, using an acyclovir prodrug where acyclovir was conjugated to chenodeoxycholate via a valine linker (4). To further evaluate prodrug approaches that exploit hASBT and to characterize the substrate requirements of hASBT, a high expressing monolayer transport assay system is needed.

Need for a Stably Transfected hASBT-MDCK System

In spite of the potential of hASBT to serve as a mechanism to enhance drug intestinal permeability, only a few efforts have targeted hASBT for this purpose (4, 5). Two related reasons underlying this circumstance appear to be a poor understanding of the substrate requirements of hASBT

Table V. Within-Day and Between-Day Variability of Taurocholate Transport Across hASBT–MDCK Monolayers Over a 6-Month Period

Parameter	Mean value	%CV	
		Within-day	Between-day
Apparent taurocholate (with sodium) permeability[a]	23.0	6.22	27.2
Taurocholate (without sodium) permeability[a]	1.30	20.3	61.7
Mannitol (with sodium) permeability[a]	2.60	11.4	72.7
Mannitol (without sodium) permeability[a]	2.40	18.9	60.3
Taurocholate V_{max}[b]	463	8.45	57.2
Taurocholate K_m[c]	14.4	15.8	48.1
Taurocholate P_p[a]	0.942	28.1	42.8

[a] Permeability units are cm/s $\times 10^6$.
[b] V_{max} units are nmol $\cdot s^{-1} \cdot cm^{-2} \times 10^6$.
[c] K_m units are μM.

(5,6) and the lack of an effective and convenient assay system to measure hASBT-mediated transport has hindered efforts. Studies probing the bile acid transporter have largely employed bile acid inhibition rather than transport assay. Our best description for hASBT substrate requirements was proposed over 25 years (16), but was based on a narrow set of solutes and utilized tissue and organs preparations from animals, including biliary excretion to assess intestinal absorption kinetics. Bile acid transport was confounded with other intestinal and hepatic transporters.

The cloning of hASBT (12,17) allows for a systematic approach to characterize hASBT's substrate requirements. Available cell culture assays employ nonpolarized cells, such as transiently transfected COS7 cells and stably transfected CHO cells. hASBT–COS7 and hASBT–CHO allow for uptake assessment, as well as uptake inhibition assessment; these cells not form competent monolayers and are unable to characterize hASBT-mediated transepithelial transport. Moreover, previous studies from our laboratory employed hASBT–COS7 cells to evaluate the hASBT kinetics of a series of bile acid conjugates of acyclovir. The cell lysis procedure complicated analysis of bile acid prodrugs, since conjugates were hydrolyzed to acyclovir (4). The hASBT–MDCK monolayer assay addresses this limitation and simplifies analytical needs.

The traditional Caco-2 monolayer assay has been used to measure bile acid transport (18–22). However, hASBT activity in Caco-2 monolayers is low and variable, resulting in an unreliable assay system. In addition, greater expression of other influx and efflux proteins in Caco-2 monolayers can confound hASBT transport. The hASBT–MDCK assay represents an approach to address these concerns, in part through high hASBT expression. In addition, inhibitors of OATP (DIDS) and MRP (probenecid) had no effect on taurocholate uptake, indicating hASBT functioning was not confounded by OATP or MRP. Bile acids are substrates for OATP and MRP (23,24).

MDCK cells were selected as a monolayer expression system since they can form competent monolayers in 4 days and have been used to study the polarized expression of membrane proteins (7,25–28). In addition, bile acid transport systems are not endogenously expressed in MDCK cells (22). This lack of hASBT expression was confirmed in our study; where both the mock transfected and wild-type MDCK cells did not exhibit carrier-mediated taurocholate transport. In addition, MDCK monolayers have been used to stably overexpress specific transporters to develop transporter-specific assay systems and thus are an appropriate choice for our model.

Characteristics of the Developed hASBT-MDCK System

High hASBT expression was observed in the developed cell line, as indicated by a 23-fold difference in taurocholate transport between transporter-mediated and passive components. This effect was further amplified in uptake assay where there was a greater than 400-fold difference. The high level of transporter activity is most advantageous, as a high passive component is known to attenuate apparent transporter activity (29). Taurocholate permeability without sodium was similar to permeabilities in mock-transfected and wild-type MDCK cells. These observations, along with low mannitol permeability, indicate that transfection and subsequent selection procedures did not alter the cell phenotype. hASBT-mediated taurocholate transport remained relatively stable over the course of the study, indicating the stability of the expressed cell line. There was relatively low between-day variability in taurocholate transport across hASBT–MDCK. However, most importantly, within day variability of taurocholate permeability was low.

The hASBT–MDCK model was developed to subsequently elucidate hASBT substrate requirements. A potential limitation of this model beyond this objective is the model's lack of a basolateral bile acid transporter(s), assuming such a transporter plays a significant role *in vivo*. The Ostα–Ostβ heterometic transporter has recently been suggested to be a basolateral bile acid carrier in the ileal and other ASBT-expressing tissues (30). MRP3 has been both supported and refuted as a mechanism of basolateral transport of bile acids in the ileum (24,31,32). In addition, a truncated version of ASBT, denoted tASBT, has been suggested as a basolateral transporter (33). The qualitative role of basolateral transporters in the transport of bile acids

across the enterocyte is still evolving. There is a lack of consensus as to the identity of a major basolateral transporter of bile acids in the ileum, if one exists. Although the hASBT–MDCK model was not designed to study basolateral kinetics, results presented here indicate that, for a high hASBT-expressing system, basolateral transport is not rate limiting. hASBT transfection lead to a 25-fold enhancement of taurocholate flux in the A–B direction, compared to control. Transport was highly polarized with a 20-fold higher flux in the A–B direction, compared to the B–A direction.

CONCLUSION

Results indicate that the developed hASBT–MDCK cell line is a valuable tool to study the interaction of native bile acids and other substrates with hASBT. This cell line will facilitate a better understanding of the substrate requirements of hASBT which would be useful in the rational design of prodrugs targeting hASBT.

APPENDIX

Modelling Approaches to Fit Taurochocolate Update and Transport Data

Fit of Taurocholate Transport Data

Two approaches were evaluated to estimate V_{max}, K_m, and P_p from taurocholate transport across hASBT–MDCK monolayers. In the first approach, P_p (i.e., passive taurocholate permeability) was estimated from sodium-free studies using Eq. (1); V_{max} and K_m were subsequently estimated from sodium-containing studies using Eq. (2). In the second approach, all three parameters were estimated simultaneously using Eq. (2), without using sodium-free transport data. Using Eq. (1), taurocholate P_p from sodium-free transport studies was 0.637 ($\pm$ 0.012) $\times 10^{-6}$ cm/s. Subsequently, V_{max} and K_m were estimated to be 1.05 ($\pm$ 0.03) $\times 10^{-3}$ nmol $\cdot$ s^{-1} cm^{-2} and 28.6 ($\pm$ 1.8) μM, respectively. Using the second approach, V_{max}, K_m, and P_p values were simultaneously estimated to be 0.937 ($\pm$ 0.085) $\times 10^{-3}$ nmol $\cdot$ s^{-1} cm^{-2}, 24.4 ($\pm$ 3.7) μM, and 0.481($\pm$ 0.368) $\times 10^{-6}$ cm/s, respectively. Each approach gave indistinguishable V_{max}, K_m, and P_p estimates from one another ($p > 0.05$). The same comparison was performed for data from six other occasions. For each occasion, the two approaches gave the same K_m estimate ($p > 0.05$). V_{max} and P_p were statistically indistinguishable, except on one occasion where the differences were not practically important. For each occasion, the second approach led to a better fit, as judged by Akaike Information Criterion (AIC). The second approach also yielded a less precise estimate of P_p, as expected since the first approach estimates P_p independently from V_{max} and K_m. Nevertheless, P_p estimates were low from either approach, particularly when evaluated against V_{max} and K_m estimates. Overall results indicate that both approaches yield practically the same kinetic parameter estimates, especially for V_{max} and K_m, which are the parameters of most interest, as these parameters characterize hASBT kinetics. Neither the first nor the second approach can be suggested as a preferred method. Rather, the selection of approach should be guided by AIC from model fit to taurocholate data in the presence of sodium.

Fit of Taurocholate Uptake Data

Similar evaluation was performed on taurocholate uptake. From sodium-free studies, P_p was estimated to be 1.88×10^{-5} cm/min. Applying this value to Eq. (2), estimates of V_{max} and K_m were 0.0208 nmol/cm^2/min and 7.27 μM, respectively. When all three parameters in Eq. (2) were simultaneously fitted to data from sodium-containing uptake studies (i.e., second approach), estimates of V_{max} (0.0181 $\pm$ 0.0011 nmol/cm^2/min) and K_m (6.00 $\pm$ 0.55 μM) were the same as those from the first approach ($p > 0.05$). Meanwhile, the P_p estimate (5.37 $\pm$ 1.20 $\times$ 10^{-5} cm/min) was about twofold higher ($p < 0.01$) than P_p from sodium-free studies. AIC values were about the same. As observed for transport studies, uptake results indicate that both approaches yield practically the same kinetic parameter estimates and that neither the first nor the second approach can be suggested as a preferred method. The decision to use either is guided by AIC from model fit to taurocholate data in the presence of sodium.

REFERENCES

1. M. H. Saier Jr. A functional-phylogenetic classification system for transmembrane solute transporters. *Microbiol. Mol. Biol. Rev.* **64**:354–411 (2000).
2. A. Ayrton and P. Morgan. Role of transport proteins in drug absorption, distribution and excretion. *Xenobiotica* **31**:469–497 (2001).
3. H. Han, *et al.* 5′-Amino acid esters of antiviral nucleosides, acyclovir, and AZT are absorbed by the intestinal PEPT1 peptide transporter. *Pharm. Res.* **15**:1154–1159 (1998).
4. S. Tolle-Sander, *et al.* Increased acyclovir oral bioavailability via a bile acid conjugate. *Mol. Pharm.* **1**:40–48 (2004).
5. B. Hagenbuch and P. Dawson. The sodium bile salt cotransport family SLC10. *Pflugers Arch.* **447**:566–570 (2004).
6. K. H. Baringhaus, *et al.* Substrate specificity of the ileal and the hepatic Na(+)/bile acid cotransporters of the rabbit. II. A reliable 3D QSAR pharmacophore model for the ileal Na(+)/bile acid cotransporter. *J. Lipid Res.* **40**:2158–2168 (1999).
7. Y. Lai, A. H. Bakken, and J. D. Unadkat. Simultaneous expression of hCNT1-CFP and hENT1-YFP in Madin-Darby canine kidney cells. Localization and vectorial transport studies. *J. Biol. Chem.* **277**:37711–37717 (2002).
8. M. A. Tanner. *Tools for Statistical Inference*, vol. 67: Lecture Notes in Statistics, Springer-Verlag, Berlin, 1992.
9. S. A. Weinman, M. W. Carruth, and P. A. Dawson. Bile acid uptake via the human apical sodium-bile acid cotransporter is electrogenic. *J. Biol. Chem.* **273**:34691–34695 (1998).
10. S. Hallen, *et al.* Membrane insertion scanning of the human ileal sodium/bile acid co-transporter. *Biochemistry* **38**:11379–11388 (1999).
11. E. Y. Zhang, *et al.* Topology scanning and putative three-dimensional structure of the extracellular binding domains of the apical sodium-dependent bile acid transporter (SLC10A2). *Biochemistry* **43**:11380–11392 (2004).
12. M. H. Wong, P. Oelkers, and P. A. Dawson. Identification of a mutation in the ileal sodium-dependent bile acid transporter gene that abolishes transport activity. *J. Biol. Chem.* **270**:27228–27234 (1995).
13. M. V. St-Pierre, *et al.* Transport of bile acids in hepatic and non-hepatic tissues. *J. Exp. Biol.* **204**:1673–1686 (2001).

14. P. Oelkers, *et al.* Primary bile acid malabsorption caused by mutations in the ileal sodium-dependent bile acid transporter gene (SLC10A2). *J. Clin. Invest.* **99**:1880–1887 (1997).
15. P. A. Dawson, *et al.* Targeted deletion of the ileal bile acid transporter eliminates enterohepatic cycling of bile acids in mice. *J. Biol. Chem.* **278**:33920–33927 (2003).
16. L. Lack. Properties and biological significance of the ileal bile salt transport system. *Environ. Health Perspect.* **33**:79–90 (1979).
17. A. L. Craddock, *et al.* Expression and transport properties of the human ileal and renal sodium-dependent bile acid transporter. *Am. J. Physiol.* **274**:G157–G169 (1998).
18. M. Kagedahl, *et al.* Use of the intestinal bile acid transporter for the uptake of cholic acid conjugates with HIV-1 protease inhibitory activity. *Pharm. Res.* **14**:176–180 (1997).
19. I. J. Hidalgo and R. T. Borchardt. Transport of bile acids in a human intestinal epithelial cell line, Caco-2. *Biochim. Biophys. Acta* **1035**:97–103 (1990).
20. C. E. Chandler, L. M. Zaccaro, and J. B. Moberly. Trans-epithelial transport of cholyltaurine by Caco-2 cell monolayers is sodium dependent. *Am. J. Physiol.* **264**:G1118–G1125 (1993).
21. K. A. Lentz, *et al.* Development of a more rapid, reduced serum culture system for Caco-2 monolayers and application to the biopharmaceutics classification system. *Int. J. Pharm.* **200**:41–51 (2000).
22. W. S. Putnam, *et al.* Functional characterization of monocarboxylic acid, large neutral amino acid, bile acid and peptide transporters, and P-glycoprotein in MDCK and Caco-2 cells. *J. Pharm. Sci.* **91**:2622–2635 (2002).
23. G. A. Kullak-Ublick, B. Stieger, and P. J. Meier. Enterohepatic bile salt transporters in normal physiology and liver disease. *Gastroenterology* **126**:322–342 (2004).
24. N. Zelcer, *et al.* Steroid and bile acid conjugates are substrates of human multidrug-resistance protein (MRP) 4 (ATP-binding cassette C4). *Biochem. J.* **371**:361–367 (2003).
25. F. R. Luo, *et al.* Intestinal transport of irinotecan in Caco-2 cells and MDCK II cells overexpressing efflux transporters Pgp, cMOAT, and MRP1. *Drug Metab. Dispos.* **30**:763–770 (2002).
26. J. W. Jonker, *et al.* Role of breast cancer resistance protein in the bioavailability and fetal penetration of topotecan. *J. Natl. Cancer Inst.* **92**:1651–1656 (2000).
27. D. Herrera-Ruiz, *et al.* A Novel hPepT1 Stably transfected cell line: establishing a correlation between expression and function. *Mol. Pharm.* **1**:136–144 (2003).
28. C. Bauch and F. Verrey. Apical heterodimeric cystine and cationic amino acid transporter expressed in MDCK cells. *Am. J. Physiol. Renal Physiol.* **283**:F181–F189 (2002).
29. K. A. Lentz, *et al.* Influence of passive permeability on apparent P-glycoprotein kinetics. *Pharm. Res.* **17**:1456–1460 (2000).
30. P. A. Dawson, *et al.* The heteromeric organic solute transporter {alpha}-{beta}, Ost{alpha}-Ost{beta}, is an ileal basolateral bile acid transporter. *J. Biol. Chem.* **280**:6960–6968 (2005).
31. T. Shoji, *et al.* ATP-dependent transport of organic anions into isolated basolateral membrane vesicles from rat intestine. *Am. J. Physiol. Gastrointest. Liver Physiol.* **287**:G749–G756 (2004).
32. D. Rost, *et al.* Regulation of rat organic anion transporters in bile salt-induced cholestatic hepatitis: effect of ursodeoxycholate. *Hepatology* **38**:187–195 (2003).
33. K. N. Lazaridis, *et al.* Alternative splicing of the rat sodium/bile acid transporter changes its cellular localization and transport properties. *Proc. Natl. Acad. Sci. USA* **97**:11092–11097 (2000).

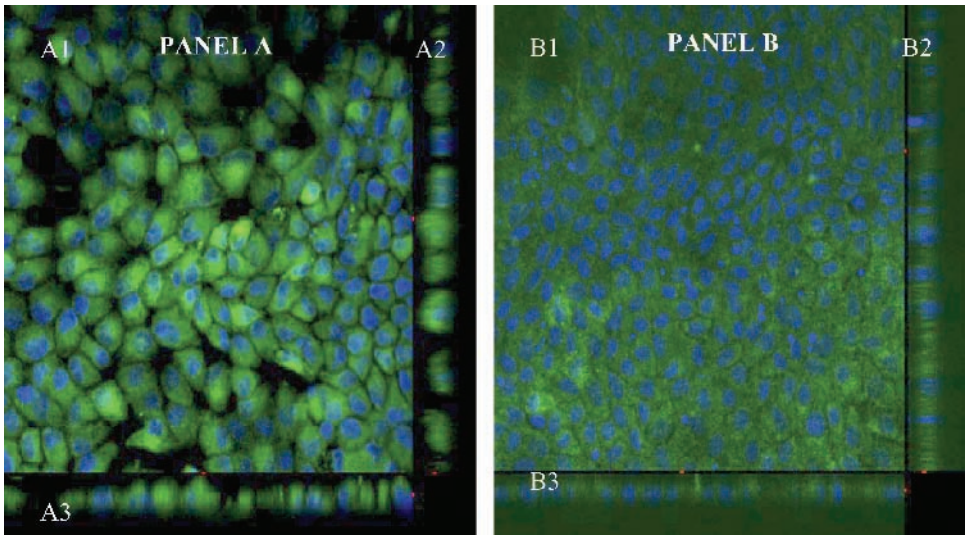

Supplementary Fig. 1. CLSM images. hASBT was stained with antibodies directed against the V-5 epitope (green). The nucleus was stained with DAPI (blue). Images were captured at 60× magnification using an oil immersion objective. Staining and image processing were the same in panels A and B. Panel A shows CLSM images of hASBT-MDCK. Images A1, A2 and A3 indicate x-y, y-z and x-z planes, respectively. ASBT was present in the apical membrane, as well as the cytosol. Panel B shows CLSM images of MDCK cells transfected with blank vector and exhibits very weak green florescence.

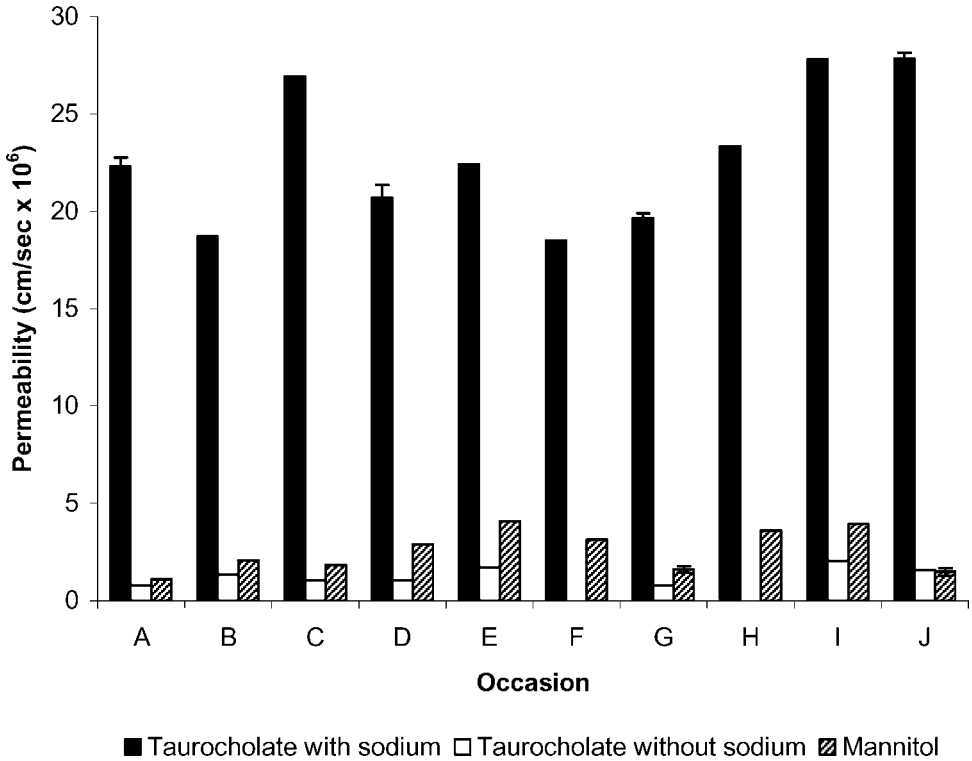

Supplementary Fig. 2. Permeabilities of taurocholate in the presence and absence of sodium on different occasions over a six month period, indicating stability of the developed hASBT-MDCK cell line. Mannitol permeabilities are also shown. The plot reflects low within day variability in taurocholate permeability, as well as relatively low between day variability in taurocholate permeability.